Development and Implementation of Biomedical Models Suitable for Modeling Microfluidic Devices

Renáta Tóthová*
Department of Software Technologies
Faculty of Management Science and Informatics
University of Žilina
Univerzitná 1, 010 26 Žilina, Slovakia
renata.tothova@fri.uniza.sk

Abstract

Currently, considerable attention is devoted to the research of blood, its features and functions of its parts. This kind of research may allow us to predict, diagnose early and treat various diseases. It is conducted in various ways, one of which is a computer (in silico) simulation. This method assumes the existence of a simulation model that simulates the behavior of the blood or blood samples in the considered environments with sufficient precision.

In this thesis, such simulation model is described, analyzed and used for specific analyses. This model allows investigation and analysis of flow of elastic objects in homogeneous fluid in microfludic devices. Microfluidic devices are used mainly for sample examination and separation or capture of cells. Our simulation model is part of the free open-source software package ESPResSo.

In this work, we describe the calibration of red blood cell model using comparison with biological experiments. Next, we present our in silico experiments leading to the optimization of microfluidic devices for effective capture of selected cells in a periodic array of obstacles. The last part of the thesis is devoted to analysis of existing methods and proposal of a new method that can be used to evaluate the damage of cells passing through a microfluidic device.

Categories and Subject Descriptors

I.6.5 [**Computing Methodologies**]: Simulation and modeling—*model development*; J.3 [**Computer Applications**]: Life and medical sciences

Keywords

spring network models, elastic objects, microfluidics, computer simulation

*Thesis supervisor: doc. Ivan Cimrák
Defended at Faculty of Management Science and Informatics, University of Žilina on August 31, 2016.

1. Motivation

In these days, the research of blood, its biological, physical or mechanical features and function of its parts is in the forefront. This kind of research may allow us to predict diagnose early and treat various diseases.

The research of blood and its features can be divided to various levels. In view of size examined particles, we have macroscopic, mesoscopic and microscopic level. The blood is homogeneous fluid on macrocsopic level, we do not see individual particles. Mesoscopic level is cell level, the blood is suspension of homogeneous blood plasma and mixture of cells. On microscopic level we see molecules and atoms, the parts of cells.

In other view, we have research in vivo, in vitro and in silico. The research with biological sample in live organism is in vivo research. Then in vitro is research with biological sample in artificial devices. Then we have young kind of research - in silico research with simulation models in computers.

In silico approach assumes the existence of a simulation model that simulates the behavior of blood or blood sample with sufficient precision. It is big challenge to create such kind of model. It may allow us to run unlimited number of simulation. Simulation model in this work is mainly for optimization of devices for testing and analyzing biological sample, capture and separation of cell and so on.

2. Simulation model

The model is able to simulate flow of elastic objects in fluid in channel with solid walls and obstacles on mesoscopic level. Dimensions of the objects are on the order μm and devices on the order tens and hundereds of μm.

2.1 Object-in-fluid modulus

Object in fluid modulus has been developed by research group Cell-in-fluid [1] as a part of software package ESPResSo [2]. This package is primarily used to simulate dynamics of many-particle systems on level of molecules and atoms.

In next part is brief description of selected part of package ESPResSo: lattice-Boltzmann method (LBM) for fluid,

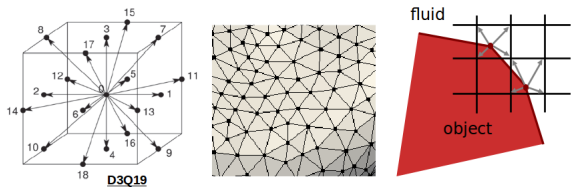

Figure 1: Parts of simulation model: regular fix lattice for fluid, irregular triangular mesh for objects and interaction objects-fluid

modulus Object-in-fluid (OIF) for elastic objects and immersed boundary method (IBM) for interaction. Schemes of these parts are on Fig. 1. Extensive description can be found in [5, 6, 14].

Fluid

Fluid is modeled by LBM [16], continuous fluid is discretized to points in fix cubic lattice. It is used D3Q19 version of LBM - the three dimensional space, 19 discrete direction e_i, where $i = 0, 1, ..., 18$, see Fig. 1.

Elastic objects

Elastic objects are deformed under the influence of external forces and they have tendency come back to original relaxed shape. The objects are covered with irregular triangular mesh of material point (nodes) see Fig. 1. The move of node is according to Newtons equations. The force, applied to the mesh node, is resulting force from all acting force - elastic force describe below and force from interactions between objects, fluid and walls.

Elastic behavior is due to 5 elastic moduli. Each modulus has own force, it depends on value of elastic coefficient and changes of object. We have stretching modulus (it depend on change of edge length between points), bending modulus (angle between adjacent triangles), modulus of constraint local area (local area of each triangle), modulus of constraint global area (global area or surface of object) and modulus of constraint global volume (global volume of object). Forces are acting in particular node of triangular mesh on object surface. All acting forces in one point are vector counted.

Interaction

Interaction between objects and fluid is modeled by IMB. It is two way interaction, objects act on fluid and fluid acts on objects. Euler's approach is used for fluid. We track a state in each node of fluid lattice. Lagrange's approach is used for objects. We track a state of moving particle (node). For describing of interaction is used so-called drag-force approach [9]. The acting of forces is interpolated to neighboring fluid or object points, see Fig. 1.

2.2 Scalability

In this part we focused on the effect of change the number of node on object surface on elastic coefficient. If we change the number of node, we change the density of mesh on object surface, too. It affects on elastic moduli. If we change the number of nodes, we do not change global area and volume. We change a little angles between triangles. But we significantly change the length of edges and local areas of triangles. We analyzed stretching modulus and modulus of conservation of local area. Based on the results of simulations, we chose the shape of these two moduli in this way to minimized sensitivity on change of point number on object surface.

2.3 $\mathcal{F}$ metric

Our model is used so-called force approach, in which we define acting forces in individual nodes. This approach is used too in [10, 19]. Different approach is so-called energy approach, in which we expect that object has zero energy in equilibrium or some energy of steady state. The object tends to minimize its energy, when some change occurs. This approach is used in models [13, 15, 18]. But in every model the formulas for energies are different. So we decided to use our force approach. We defined $\mathcal{F}$ metrics for easy evaluation what proportion of deformation belongs to particular elastic modulus. Let us denote vertex of triangle (node) as ν and acting stretching force in this vertex ν from edge e_i as $\mathbf{F}_s(e_i)$. Then the contribution from stretching modulus in this node $\widetilde{\mathbf{F}}_s(\nu)$ is calculated as vector sum of the individual stretching forces. The contribution from stretching modulus from whole object $\mathcal{F}_s$ is calculated as sum individual contributions $\widetilde{\mathbf{F}}_s(\nu)$. The same method we use for other elastic modulus. The total value $\mathcal{F}$ is calculated as sum of contributions from individual modulus.

We performed several simulations, in which we deformed sphere in different ways and we track the values of individual $\mathcal{F}$ metrics. The result allow us to used $\mathcal{F}$ metric as energy-like quantity for quality evaluation energy state of object. The graphics interpretation contributions of $\mathcal{F}$ metric give us the information about local state on object surface.

3. Model of red blood cell

One of the main fields of applications of our model is modeling of flow red blood cell (RBC) in microfluidic devices. It is important, that shape of the model RBC and elastic behavior was similar or comparable to biological RBC.

3.1 Biological RBC and its model

RBC are important, highly specialized blood cells. They are found in the blood of all vertebrates and their main purpose is to transport oxygen from the lungs to the tissues and carbon dioxide back from the tissues to the lungs.

On the Fig. 2 left is shown cut of RBC with average dimensions. Our model models only membrane RBC. Part of membrane is lipid bilayer with mesh of several proteins, which create some supporting structure of the membrane. They are responsible for elastic behavior of cell. The main protein of this mesh is spectrin. We can imagine it as a network of springs on the membrane surface, which can stretch, press and bend under the external forces. If they are no acting force, mesh of springs comes back the membrane to original relaxed shape. The describe of mechanical and rheological properties of RBC is, for example, in [3, 4].

Biconcave shape of RBC is described by analytical function in [11]. Mostly in our simulation, we are using model of RBC, which was created by covering the surface (based on analytical function) with triangles, see Fig. 2 right. Individual objects we can generate on different position,

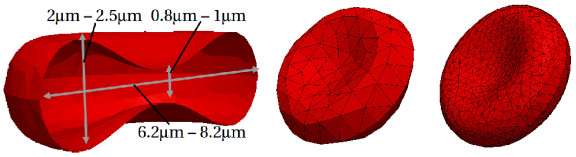

Figure 2: On the left is cut of RBC membrane with average dimensions of biological RBC. On the right is model RBC with 141 and 786 nodes on surface.

with different rotation and thus simulate random distribution of cells in fluid. Depending on the number of nodes on surface vary the geometric parameters of models.

3.2 Analysis behavior of cell in shear flow

The motivation for this study was information in [12]. If the surface of RBC increases by 4%, the immediately membrane destruction occurs. If the surface increases by 2% in longterm, teh membrane destruction occurs also. We were interested in, what will happen on local level. How will the local area of individual triangle change?

The proposal of simulation is on Fig. 3. We ran several simulations with different starting rotation of cell and different flow velocity, it means with different shear stress τ. Also we changed elastic coefficient for constraint global area k_{ag}.

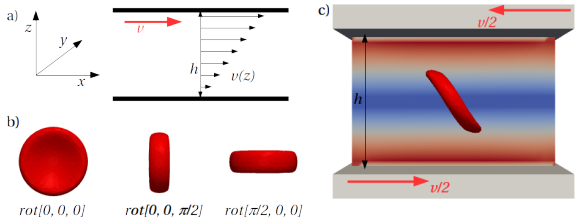

Figure 3: In a) is scheme of Couette flow in channel, where top plate is moving with velocity v and bottom plate is not moving. Inside the channel, the flow velocity is function of hight z. In b) are shown selected rotation of RBC and their marks. In c) is simulation scheme of RBC in shear flow. Both plates are moving in opposite direction with velocity $v/2$. The color of fluid corresponds with its velocity from maximum near the plate (red) to minimum in the middle (blue).

We have following results from the simulations. In general, cell is rapidly stretched at the beginning of simulation. The critical value of surface increase is achieved in different time with different shear stress for different starting rotation of cell. Next the stretch (or strain) oc dell decreases and cell starts to rotate in flow. The relative areal strain is periodically changing. If the stiffness of cell increases (k_{ag} increases), we need greater shear stress to achieve same areal strain. The dependence of critical shear stress (with critical strain) on k_{ag} is nearly linear. So the greater shear stress means greater areal strain, respectively deformation. With greater shear stress the areal strain is greater and achieves sooner.

Subsequently, we analyzed local strain of individual triangles on the surface. However, that global strain of cell achieved 4%, local parts of surface were stretched significantly more. We recorded several triangles with more then 100% increase compared to the original area. We defined cumulative membrane damage Υ. In this damage, we consider size and duration of strain. On Fig. 4 shape of cell is shown at the beginning of simulation and at the moment of critical areal strain. This moment occurs in different time for different cell rotation. Direction of fluid flow is depicted with red arrows. The coloring of membrane represents the value Υ for individual triangles from the blue lowest to red highest. In this way, we know to localize the most stretched (deformed) region.

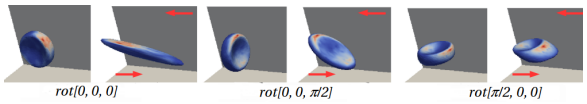

Figure 4: For each starting rotation of cell is given picture for its shape at the beginning of simulation and at the moment of critical areal strain. Colors correspond to value Υ for individual triangle, the lowest is blue and the highest is red. Direction of fluid flow is depicted with red arrows.

3.3 Calibration of RBC model

For calibration of RBC model we used so-called stretch experiment with biological RBC, which is describe in [7]. Briefly say: biological cell was stretched known force and was measured change of diameters, see Fig. 5.

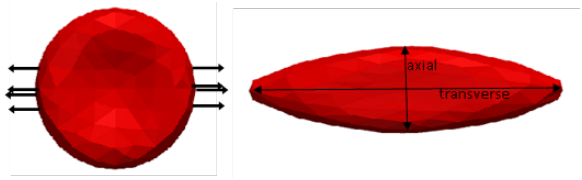

Figure 5: On the left, we see the beginning of simulation, the cell is stretched by applying force at several nodes on surface (black arrows). On the right is final stage of simulation - relaxed state, we measured transversal and axial diameter.

In our model we chose set of 5 values of elastic coefficients and cell stretched known force. When the cell stopped motion (it was in equilibrium), we wrote the values of axial and transversal diameter. This step we repeated for different force and we wrote the results to graph as a dependency of diameter changes on applied force. Subsequently we repeated simulations for different set of coefficients. We compared results with experimental data. We used sum of squared errors SE for quantitative evaluation, how good is fit simulation data with experimental data. This procedure we repeated for various set of elastic coefficients and we found set with minimal error SE.

We calibrated model RBC with 141 and 786 nodes on surface with this procedure. Base on two sets calibrated coefficients we calculated by linear interpolation coefficients for model with 374 and 670 nodes.

We analyzed the sensitivity of individual coefficients on change. From results we found out, that model is very sensitive on change of coefficients k_s (stretching modulus) k_b (bending modulus) in comparing with others coefficients.

On the left on Fig. 6 is graph dependency measured diameters of cell on applied force for model with 141 and 786 nodes for set of elastic coefficient with minimal SE. We see very good fit with experimental data. On the right is table with SE from stretched simulations for different values of coefficients k_s and k_b, predicted value is in the middle of table in region of green the lowest values SE.

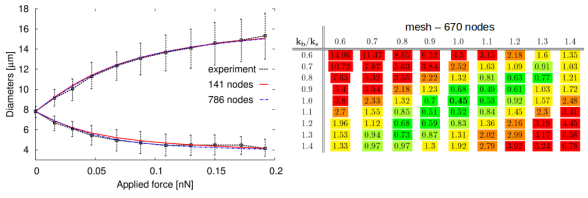

Figure 6: On the left dependency change of diameters on applied external force. Shown are results from experiment with error bars and measured values from simulations with model with 141 and 786 nodes. Depicted lines are for minimal achieved values SE for given model. On the right are values SE for combinations of multiples of predicted values of elastic coefficient for model with 670 nodes. Color of items is changed from red - the greatest errors to green - the lowest errors. Predicted value is in the middle of table.

4. Application of OIF modulus

In the following chapters are presented two studies, which showing possibilities of our model. We have the ambition, the model has been available in practice for relative quick and cheap studies about design (geometry) microfluidic device for the purpose their optimization. The speed depend on processing power available computers or cluster of computers. The cheap price means, that for this type of studies we do not need to made given device and to create sample of fluid. Together, it is possible run many repeating and changing of simulations.

4.1 Cell flow in periodic array of obstacles

In this study we considered microfluidic device, in which is the periodic array of obstacles. In this case, the obstacles are columns and they are repeated periodically, see Fig. 7, left. On the right there is scheme of simulation box with periodic boundary conditions.

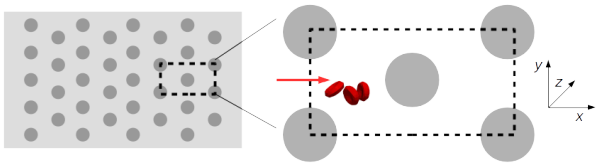

Figure 7: On the left is scheme of periodic array of obstacles and selected simulation box. On the right is scheme of simulation box, arrow shows the direction of flow, black dotted lines show boundary of box with periodic boundary condition.

In this study, we focused on confirmation of the hypothesis that higher density of cells in the sample affects the trajectory of CTC (circulating tumor cells) in the device. Thus also that, it affects the capture of these cells. Finally we proposed a model to estimate the measure of cells capture rate.

To estimate of cell capture rate P_a, we proposed simplified formula, based on the work [8]: $P_a(\tau, A_c) = aA_c \exp\left[-b\frac{\tau}{A_c}\right]$, where A_c is size of interaction area between cell and functionalized surface, τ is shear stress in flow, a and b are constants, which can be determined empirically from the experiment for a particular type of cells and surfaces, example is the study [20].

We ran simulation for 4 different diameters of columns (obstacles) - 7, 9, 11, 13μm, with 3 different numbers of cells - 10, 50, 100 and for 10 different initial position of CTC at the beginning of simulation box ($x = 1\mu m$).

We received more data. On Fig. 8 is depicted, how RBC affect movement of CTC. With 10 RBC (left), the effect is minimal, but with 100 RBC (right) we see changes in trajectories. Similarly we studied movement of individual RBC, too.

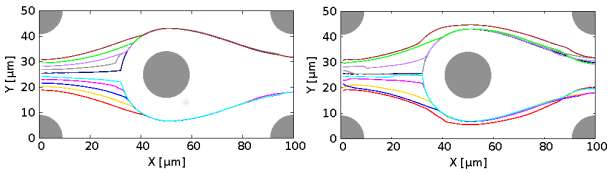

Figure 8: Typical trajectories of CTC in simulations with 10 RBC on the left and with 100 RBC on the right. Each lines correspond with position of CTC centroid with different starting position.

In the next step we were interested in estimation of cell capture rate. We focused on qualitative evaluation of individual configuration - 4 different diameters of obstacles / columns and 3 different number of cells. For each configuration and initial position of CTC we ran 10 simulations, in each simulation the initial position of RBC was randomly set. We defined vector of initial positions of CTC and to its vector of end positions. The end positions, we evaluated by weight, depending on how often the cell itself in the end position. Individual end positions were initial position of next pass trough the box - next iteration. The number of iterations is responsible to number of pass trough simulation box, respectively the size of device.

The results from measured and calculated values are as follows. The capture rate increases with increase number of cell. Probably, CTC is more often near to column. On the other hand, the capture rate decreases with greater diameter of columns. In this case, probably, it is important fact, that they is to little space for cell in the box. So RBC can push CTC to columns, but in the same time RBC can be between CTC and column and keep CTC from the touch.

4.2 Optimization of microfluidic device in view of cell damage

In this study we focus on analysis of cell behavior, when the cells pass micro channel. Result from such kind of simulations can help in design of device in way of minimizing cell damage.

The [17] and [21] were main motivation. The authors wrote about so-called blood damage index BDI. For chosen geometry, this index is calculated as sum of local shear stress along fluid streamlines inside the device. It is used

to evaluate possible mechanical stress, which causes deformation, damage or destruction of cell.

Our simulation model provides information about change of individual objects in fluid flow. We were interested in extended damage index - cell damage index CDI. In this index will be included mutual interaction between cells, fluid and walls of device.

For estimation the cell damage, we defined next variables. Cumulative deviation of global area $CDG(cell) = \sum_{time} \frac{|S-S_0|}{S_0}$ for one cell, where $time$ is period, during which the cell pass through monitored region of channel, S is actual global area of cell, S_0 is original area of cell and $\frac{|S-S_0|}{S_0}$ is immediate absolute relative change of global area. This variable is computed for all tracking cells in given simulation. Next average cumulative deviation of global area $CDG_{simNo} = \frac{1}{n_{cell}} \sum_{cell} CDG(cell)$, where n_{cell} is number of cells in simulation, for which we track $CDG(cell)$. Finally we defined extended CDI as arithmetic mean of CDG_{simNo} from one set od simulations. These simulations were different in position of cell at the beginning of simulations. $CDI = \frac{1}{N} \sum_{simNo} CDG_{simNo}$, where N is number of simulation in one set, from which we calculated the index.

The following analysis is used to check the presumption, that defined CDI can be used to estimate the cell damage.

4.2.1 Analysis of proposed damage index

We chose 4 different geometries, see Fig. 9. The channels are different from each other in middle part. It has various bend or curvature. But the cross section stays same - square $40\mu m \times 40\mu m$.

For each channel, we ran set of 10 simulations. The simulations in one set have same number of cell, but with different starting positions and rotations. We ran sets of simulations with 10, 30 and 50 cells. For channel 3 we ran sets with 60, 70, 80 and 90 cells, too.

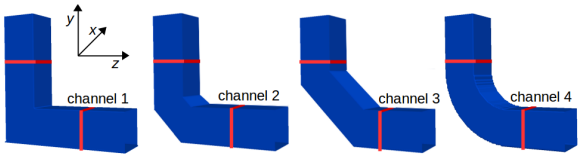

Figure 9: Design of channel geometries for testing the proposed CDI. The square cross section is the same in each channel. The region of interest is depicted with red lines.

Calculated values CDI with standard deviation σ are in Tab. 1. Deviation σ was calculated from values CDG_{simNo}.

CDI increases with number of cell in channel. In denser flow, mutual cell interactions occur more frequently, due to it to their deformations too. From the table, we see. that $CDI(kanál\,1) < CDI(kanál\,2) < CDI(kanál\,3)$ for sets with 30 and 50 cells. The cell damage is smaller with "smoother"bend of channel. For sets with 10 cells, flow is probably thin enough, so cells are moving along ideal trajectories with minimal deformation, whether a channel bend.

On the other hand, $CDI(kanál\,4) > CDI(kanál\,3)$, whether channel 4 is smoother then channel 3. Probably, in this case, it is important the length of trajectory, because $CDG(cell)$ is summed during the cell passes the channel.

Table 1: Values of CDI and standard deviation σ for individual set of simulations. The number of cells is changed in columns, the type of channel is changed in lines.

	number of cells						
CDI	10	30	50	60	70	80	90
ch 1	0.09	0.12	0.15				
σ	0.02	0.01	0.01				
ch 2	0.09	0.11	0.14				
σ	0.03	0.01	0.01				
ch 3	0.08	0.1	0.13	0.14	0.16	0.17	0.19
σ	0.02	0.01	0.01	0.01	0.01	0.01	0.01
ch 4	0.07	0.11	0.13				
σ	0.01	0.01	0.01				

The deviation σ roughly decreases with increase of cell, so when number of cell increases, dispersion of CDG_{simNo} decreases.

In Tab. 2 we compared primary BDI with our CDI. The table has 2 parts. In first part, there are values of CDI for sets of simulations with 50 cells. In second part, there are values of BDI for given channels. For better view, values of BDI are multiply by $\times 10^5$.

In first column are calculated values CDI and BDI for each channels, next the ratio to reference value (as reference value we took value for channel 1). The difference between channel 1 and 2 is same for CDI and BDI, but distance between channels 1, 2 and 3, 4 is greater for BDI.

Table 2: Values CDI and BDI for channels 1, 2, 3 and 4 and their ratio to reference values. Then they are maximal achieved values $CDG(cell)$ from all cells in set and from all partial BDI.

channel	CDI	$\frac{CDI}{CDI_{ref}}$	max	$\frac{max}{CDI}$	$\frac{max}{max_{ref}}$
1	0.1480	1.000	0.3879	2.621	1.00
2	0.1380	0.932	0.4088	2.962	1.05
3	0.1294	0.874	0.4366	3.374	1.13
4	0.1320	0.892	0.3984	3.018	1.03
kanál	BDI	$\frac{BDI}{BDI_{ref}}$	max	$\frac{max}{BDI}$	$\frac{max}{max_{ref}}$
1	2.4355	1.000	6.006	2.466	1.00
2	2.2762	0.935	5.8453	2.568	0.97
3	1.9844	0.815	5.5478	2.796	0.92
4	2.0267	0.832	5.624	2.775	0.94

4.2.2 Influence of flow density to damage

In previous chapter we presented simulation, in which the cells was placed only at the beginning of channel. In next step we placed the cell randomly in whole volume of channel. For comparing influence of flow density, respectively number of cells in channel (hematocrit) on cell damage, we ran three sets of simulation in channel 1, see Fig. 10.

In Tab. 3, there are outcomes for simulations with hematocrit 5%, 10% a 15%. When hematocrit increases,

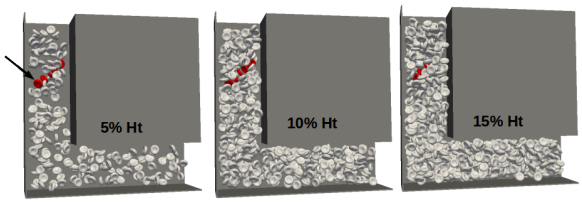

Figure 10: Snapshots from simulations with hematocrit 5%, 10% a 15%. Black arrow shows cell, which data is on Fig.

CDI increases two and in the same time dispersion of CDG_{simNo} decreases. It means, that with greater hematocrit in simulation, we need less simulations to achieved sufficient accuracy of CDI.

Table 3: Values CDI for channel 1 for hematocrit 5%, 10% a 15% and their ratio to reference values. Then they are standard deviation σ calculated from 10 values CDG_{simNo} and their ratio to CDI. In next columns they are maximal achieved values from all CDG_{simNo}.

ch 1	CDI	$\frac{CDI}{CDI_{ref}}$	σ	$\frac{\sigma}{CDI}$	max	$\frac{max}{CDI}$
5%	0.185	1.00	0.015	0.08	0.21	1.13
10%	0.278	1.50	0.017	0.06	0.302	1.09
15%	0.360	1.95	0.007	0.02	0.369	1.02

Individual values of $CDG(cell)$ for all tracked cells are processed in histograms on Fig. 11 left. Histograms are normalized to number of cell in individual sets od simulations. With greater hematocrit, the maximal frequency was achieved for greater value of $CDG(cell)$ and in same time was achieved greater maximal value. We conclude, that greater hematocrit it leads to greater cell deformation.

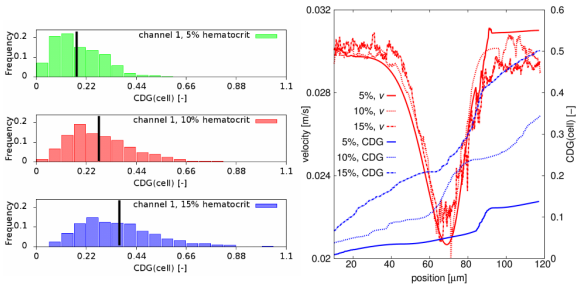

Figure 11: On the left histograms for channel 1, hematocrit 5% (green), 10% (red) and 15% (blue). On x-axis are achieved values $CDG(cell)$. On y-axis is frequency of cells from given interval, normalized to total cell number from the set of simulations. On the right is dependency of cell velocity on position in channel for chosen cell for hematocrit 5%, 10% a 15% - red lines. With blue lines are depicted dependency of $CDG(cell)$ for chosen cell on position in channel.

In next step we performed analysis of cell velocity and $CDG(cell)$ for given cells. We ran 3 simulations, each with different hematocrit. Th given cell was in the same position and rotation at the beginning of simulation in each simulation. Other cells was randomly seeded with given hematocrit.

Velocities and trajectories of cells are comparable. The $CDG(cell)$ are different significantly, what is illustrated in graph on Fig. 11, right. Dependency of actual cell velocity on position in channel is depicted with red. Coordinates of initial position of cell were $(19\mu m, 88\mu m, 11\mu m)$. The lines are differ from each other only slightly, mainly in particular local fluctuations. These fluctuations are caused by interaction between cells. If the cells are closer to each other at a distance less than the set value, the cells begin to repel. At the same time the speed of cell is calculated as the average speed of all nodes on its surface. These two factors may cause, that we see smooth flow of cell in simulations and in detail view we see steep, but small, changes in direction and magnitude of velocity.

Lines for $CDG(cell)$ are depicted with blue on the graph. As we expected, cumulative value of relative deviation global area increases with time, respectively with traveled distance. In general, $CDG(cell)$ is depended on position, trajectory and surrounding of given cell. Surrounding means other cells and obstacles. The $CDG(cell)$ is greater with greater hematocrit. This applies to most of cells, as we see in histograms on the left.

In Tab. 4 are values CDI and BDI for different hematocrit together with ratio to reference value. Greater differences are for CDI in comparing with BDI, but the trend is same for both indexes.

Table 4: Values CDI and BDI for channel 1 for hematocrit 5%, 10% a 15% and their ratio to reference value.

ch 1	CDI	$\frac{CDI}{CDI_{ref}}$	BDI	$\frac{BDI}{BDI_{ref}}$
5%	0.1851	1.000	0.3259	1.000
10%	0.2783	1.504	0.3694	1.133
15%	0.3603	1.946	0.4205	1.29

From these data we can conclude, that we know qualitative evaluation individual geometries - channels with our CDI. These evaluations are not significantly different from BDI. But we have extra information about damage of individual cells.

Next, it will be appropriate to preformed a similar simulation for channel 3 and 4 and for greater hematocrit, too. Then we will compute and compare values CDI a BDI for real geometries and outcomes will be compare with experiments.

5. Conclusion

In this work is closer described device for the analysis of cells in a blood sample. The parameters of these devices directly affect their properties, such as the efficiency of detection, identification of the selected cells or damage. Testing these devices in vitro is relative finance and time consuming. Simulation in silico can give answers to many questions much faster and cheaper. The prerequisite, however, is to have a good simulation model.

This work is devoted to the description, development and use of simulation model. This model can be used to simulate the flow of cells in a homogeneous environment in artificial devices. This model is produced as part of the research of the Cell-in-fluid [1].
The main contribution of this work include: - proposal, analysis and implementation of the new shape of the stret-

ching modulus and the modulus constraint local area.
- calibration of model RBC - proposal of calibration algorithm and its performance for model with different number of nodes.
- proposal and realization of simulations in silico, which used the simulation model for analysis of behavior of cell flow in fluid. The model was used for analysis the capture rate of selected cells in devices depends on device geometry and sample density. Next it was proposed a new approach for evaluation of geometry in view of cell damage. This approach has been tested and analyzed in several views with amount of series of simulations.

References

[1] Cell-in-fluid research group. http://cell-in-fluid.fri.uniza.sk. online, prevzaté: apríl 2016.

[2] A. Arnold, O. Lenz, S. Kesselheim, R. Weeber, F. Fahrenberger, D. Roehm, P. Košovan, and C. Holm. ESPResSo 3.1 — Molecular dynamics software for coarse-grained models. In M. Griebel and M. A. Schweitzer, editors, *Meshfree Methods for Partial Differential Equations VI*, volume 89 of *Lecture Notes in Computational Science and Engineering*, pages 1–23. Springer, 2013.

[3] O. K. Baskurt. *Handbook of hemorheology and hemodynamics*. IOS Press Inc., 2007.

[4] D. Boal. *Mechanics of the Cell*. Cambridge University Press, 2001. Cambridge Books Online.

[5] I. Cimrák, M. Gusenbauer, and I. Jančigová. An ESPResSo implementation of elastic objects immersed in a fluid. *Computer Physics Communications*, 185(3):900–907, 2014.

[6] I. Cimrák, I. Jančigová, R. Tóthová, and M. Gusenbauer. Mesh-based modeling of individual cells and their dynamics in biological fluids. In R. Bris, J. Majernik, K. Pancerz, and E. Zaitseva, editors, *Applications of Computational Intelligence in Biomedical Technology*, volume 606 of *Studies in Computational Intelligence*, pages 1–28. Springer International Publishing, 2015.

[7] M. Dao, J. Li, and S. Suresh. Molecularly based analysis of deformation of spectrin network and human erythrocyte. *Materials Science and Engineering: C*, 26(8):1232–1244, 2006.

[8] P. Decuzzi and M. Ferrari. The adhesive strength of non-spherical particles mediated by specific interactions. *Biomaterials*, 27(30):5307–5314, 2006.

[9] B. Dunweg and A. J. C. Ladd. Lattice-Boltzmann simulations of soft matter systems. *Advances in Polymer Science*, 221:89–166, 2009.

[10] M. Dupin, I. Halliday, C. Care, and L. Alboul. Modeling the flow of dense suspensions of deformable particles in three dimensions. *Phys Rev E Stat Nonlin Soft Matter Phys.*, 75, 2007.

[11] E. Evans and Y.-C. Fung. Improved measurements of the erythrocyte geometry. *Microvascular Research*, 4(4):335–347, 1972.

[12] E. Evans, R. Waugh, and L. Melnik. Elastic area compressibility modulus of red cell membrane. *Biophysical Journal*, 16(6):585–595, 1976.

[13] D. A. Fedosov, B. Caswell, and G. E. Karniadakis. A multiscale red blood cell model with accurate mechanics, rheology, and dynamics. *Biophysical Journal*, 98(10):2215–2225, 2010.

[14] I. Jančigová. *Modeling elastic objects in fluid flow with biomedical applications*. PhD thesis, University of Žilina, 2015.

[15] T. Kruger, M. Gross, D. Raabe, and F. Varnik. Crossover from tumbling to tank-treading-like motion in dense simulated suspensions of red blood cells. *Soft Matter*, 9(37):9008–9015, 2013.

[16] A. J. C. Ladd. Numerical simulations of particulate suspensions via a discretized Boltzmann equation. Part 2. Numerical results. *Journal of Fluid Mechanics*, 271:311–339, 6 1994.

[17] H. Li, X. Ruan, W. Qian, and X. Fu. Numerical estimation of hemolysis from the point of view of signal and system. *Artificial Organs*, 38(12):1065–1075, 2014.

[18] M. Nakamura, S. Bessho, and S. Wada. Spring network based model of a red blood cell for simulating mesoscopic blood flow. *International journal for numerical methods in biomedical engineering*, 29(1):114–128, 2013.

[19] T. Omori, T. Ishikawa, D. Barthès-Biesel, A.-V. Salsac, J. Walter, Y. Imai, and T. Yamaguchi. Comparison between spring network models and continuum constitutive laws: Application to the large deformation of a capsule in shear flow. *Phys. Rev. E*, 83:041918, Apr 2011.

[20] S. Santana, H. Liu, N. Bander, J. Gleghorn, and B. Kirby. Immunocapture of prostate cancer cells by use of anti-psma antibodies in microdevices. *Biomedical Microdevices*, 14(2):401–407, 2012.

[21] M. E. Taskin, K. H. Fraser, T. Zhang, C. Wu, B. P. Griffith, and Z. J. Wu. Evaluation of Eulerian and Lagrangian models for hemolysis estimation. *Asaio Journal*, 58(4):363–372, 2012.

Selected Papers by the Author

Jančigová, I., Tóthová, R. Scalability of forces in mesh-based models of elastic objects. In *ELEKTRO 2014: 10th International Conference*, IEEE, pp. 562-566, 2014, ISBN 978-1-4799-3720-2.

Tóthová, R., Jančigová, I., Cimrák, I. Energy contributions of different elastic moduli in mesh-based modeling of deformable object. In *ELEKTRO 2014: 10th International Conference*, IEEE, pp. 634-638, 2014, ISBN 978-1-4799-3720-2.

Cimrák, I., Jančigová, I., Tóthová, R. Recent advances in mesh-based modeling of individual cells in biological fluids. In *Digital technologies: the 10th international conference*, IEEE, pp. 25-31, 2014, ISBN 978-1-4799-3301-3

Tóthová, R., Jančigová, I., Bušík, M. Calibration of elastic coefficients for spring-network model of red blood cell. In *Information and Digital Technologies (IDT) 2015, International Conference*, IEEE, pp. 376-380, 2015, ISBN 978-1-4673-7185-8

Tóthová, R., Cimrák, I. Local stress analysis of red blood cells in shear flow. In *AIP Conference Proceedings*, Vol. 1648, eid: 210003, 2015, ISBN 978-0-7354-1287-3

Cimrák, I., Jančigová, I., Tóthová, R., Gusenbauer, M Mesh-based modeling of individual cells and their dynamics in biological fluids. , R. Bris, J. MAjernik, K. Pancerz, E. Zaitseva, eds. In *Applications of Computational Intelligence in Biomedical Technology, vol. 606 of Studies in Computational Intelligence*, Springer International Publishing, 2015, ISBN 978-3-319-19146-1

Cimrák, I.. Bachratá, K., Bachratý, H., Jančigová, I., Tóthová, R., Bušík, M., Slavík, M., Gusenbauer, M. Object-in-fluid framework in modeling of blood flow in microfluidic channels. In *Comunications, Scientific Letters of the University of Žilina*, vol. 18/1a, pp. 13-20, 2016, ISSN 1335-4205